A comparative study of the structure and energetics of elementary defects in 3C- and 4H-SiC

2004 J. Phys.: Condens. Matter 16 1307

(http://iopscience.iop.org/0953-8984/16/8/015)

INSTITUTE OF PHYSICS PUBLISHING JOURNAL OF PHYSICS: CONDENSED MATTER

J. Phys.: Condens. Matter **16** (2004) 1307–1323 PII: S0953-8984(04)69813-4

A comparative study of the structure and energetics of elementary defects in 3C- and 4H-SiC

M Posselt[1,4], F Gao[2], W J Weber[2] and V Belko[3]

[1] Forschungszentrum Rossendorf, Institute of Ion Beam Physics and Materials Research, PO Box 510119, D-01314 Dresden, Germany
[2] Fundamental Science Directorate, Pacific Northwest National Laboratory, PO Box 999, Richland, WA 99352, USA
[3] Department of Mathematical Physics, Belarus State University, F Skorina Avenue 4, 220050 Minsk, Belarus

E-mail: M.Posselt@fz-rossendorf.de

Received 1 October 2003
Published 13 February 2004
Online at stacks.iop.org/JPhysCM/16/1307 (DOI: 10.1088/0953-8984/16/8/015)

Abstract

The potential non-equivalent defects in both 3C- and 4H-SiC are classified by a new method that is based on symmetry considerations. In 4H-SiC their number is considerably higher than in 3C-SiC, since the hexagonal symmetry leads to diversification. The different theoretical methods hitherto used to investigate defects in 3C-SiC are critically reviewed. Classical MD simulations with a recently developed interatomic potential are employed to investigate the stability, structure and energetics of the large number of non-equivalent defects that may exist in 4H-SiC. Most of the potential defect configurations in 4H-SiC are found to be stable. The interstitials between hexagonal and trigonal rings, which do not exist in 3C-SiC, are characteristic for 4H-SiC and other hexagonal polytypes. The structure and energetics of some complex and anisotropic dumbbells depend strongly on the polytype. On the other hand, polytypism does not have a significant influence on the properties of the more compact and isotropic defects, such as vacancies, antisites, hexagonal interstitials, and many dumbbells. The results allow conclusions to be drawn about the energy hierarchy of the defects.

1. Introduction

Silicon carbide (SiC) is a promising material for applications in power devices and high temperature electronics. Ion implantation is considered to be the best means for selective electrical doping of SiC. However, ion irradiation produces defects that can prevent the electrical activation of the implanted dopants. The knowledge of ion-beam-induced defect formation and evolution in SiC is therefore very important, and much of the understanding

[4] Author to whom any correspondence should be addressed.

will be derived from the results of investigations of elementary defects, such as vacancies, antisites and self-interstitials. The available data on defect stability, formation energy and structure at absolute zero (0 K) have mostly been obtained by theoretical studies that consider the relaxation of a computational cell containing a small volume of SiC that includes the initial configuration of the defect under consideration. The driving forces for the relaxation are obtained by either taking into account both electronic and ionic degrees of freedom or considering the lattice atoms as elementary units. In the first and second cases, the interactions are determined by *ab initio* methods and by classical interatomic potentials, respectively. The latter methods are limited to neutral defects whereas the former are also able to investigate the influence of electrical charges. The relaxation procedure itself consists of either energy minimization by known numerical recipes or rapid quenching in the framework of molecular dynamics (MD) simulations. A peculiarity of SiC is the occurrence of polytypism with more than 200 different polytypes. Because of its simple lattice structure, previous investigations on elementary defects were mostly focused on the cubic 3C polytype of SiC. On the other hand, SiC wafers for technological applications are either of 4H or 6H polytype. It is therefore very important to extend the theoretical investigations on elementary defects to these more complicated crystal structures.

In the present work, a comparative study of neutral vacancies, antisites and self-interstitials in 4H- and 3C-SiC at 0 K is performed. Section 2 gives a short overview on lattice structure and suitable geometrical representation of both polytypes. Using symmetry considerations, the potential defects are classified in section 3. These defect configurations define the initial condition for the relaxation of the computational cell. In the literature, different definitions have been used for the formation energies of defects in the binary SiC system. This renders the comparison between previous results more difficult. Therefore, some clarification on this topic is provided, even though it largely represents known concepts (cf section 4). The available theoretical data on the structure and energetics of defects in 3C-SiC are critically reviewed. MD simulations are employed to calculate the properties of elementary defects in 3C- and 4H-SiC (cf section 5) using the classical interatomic potential developed by Gao and Weber [1]. The application of this method is justified since the present comprehensive comparative study aims to provide a first and relative estimate of the influence of polytypism on stability, formation energy and structure of elementary defects. Furthermore, the use of classical potentials has the important advantage that it requires much less computational effort than *ab initio* calculations.

2. Polytypism of SiC

The following short overview on structure and suitable geometrical representation of different SiC polytypes is limited to supporting the objectives of this work. For a detailed description of crystal symmetry, structure, and polytypism, the reader is referred to previous literature [2–4]. The lattice structure of SiC is characterized by fourfold-coordinated Si and C arranged in tetrahedra. In all polytypes, the atoms have identical nearest neighbours. However, there are differences in the second, the third, and the following neighbour shells. Each polytype can be characterized by a certain stacking sequence of layers of tetrahedra along a direction parallel to Si–C bonds whose orientations are identical in all layers. This direction is called the c-axis, and the plane perpendicular to the c-axis is the basal plane. In the stack, the layers may differ in the orientation of those Si–C bonds that are not parallel to the c-axis. 3C-SiC is the only cubic polytype, and the periodicity of stacking is three. The other polytypes show hexagonal and rhombohedral symmetry. For example, 6H-SiC is a hexagonal polytype where the periodicity of stacking is six; in the rhombohedral polytype, 15R-SiC, the periodicity is 15. In the hexagonal and rhombohedral polytypes, slight deviations from the ideal tetrahedral

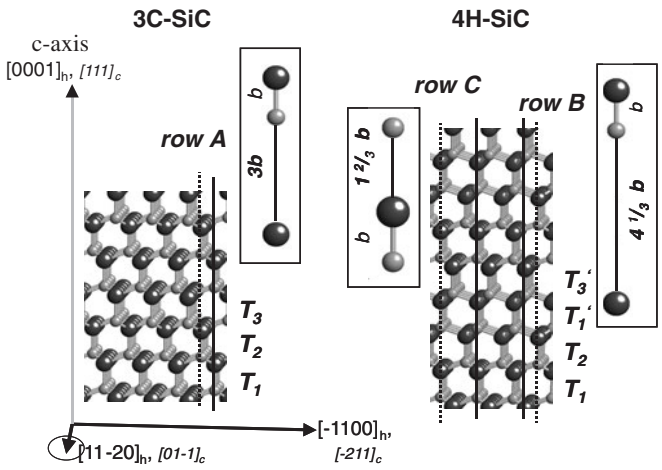

Figure 1. The lattice structure of 3C- and 4H-SiC. The crystal axes are given in hexagonal and cubic notation. Silicon and carbon atoms are depicted by larger dark and smaller grey spheres, respectively. A polytype may be characterized by a certain stacking sequence of layers of tetrahedra along the c-axis. In 3C- and 4H-SiC the periodicity of stacking is three and four, respectively. T_1, T_2, T_3, T_1', and T_3' denote different types of layers. The lattice can be also constructed by a two-dimensional periodic arrangement of the intersections of Si–C dimer rows with the basal plane, where the rows are perpendicular to this plane. Whereas in 3C-SiC only one type of dimer rows (A) exists, there are two different rows (B and C) in 4H-SiC. The solid and dotted lines show rows with different coordinates relative to the axis [11–20]. The insets depict the dimer sequences in rows A, B and C in detail. The nearest neighbour distance is denoted by b. It is used as unit of the distance between two dimers. Note that this and the following figures show only a part of the crystal. Therefore, not all bonds of the atoms are drawn.

structure exist. These are neglected in following considerations. Figure 1 illustrates the stacked layers of CSi_4 (or SiC_4) tetrahedra in the cases of 3C- and 4H-SiC. The crystal axes are given in hexagonal and cubic notations. Another possibility to characterize the polytypism is based on the consideration of Si–C dimer rows that are perpendicular to the basal plane. The lattice can be built by a two-dimensional periodic arrangement of the intersections of these dimer rows with the basal plane. The rows may differ in the arrangement of the dimers. In 3C-SiC only one type of dimer rows, called *row A*, exists. Therefore, the number of non-equivalent Si and C sites is one. In 4H-SiC there are two different rows, namely rows B and C. This leads to two non-equivalent sites for both Si and C. The insets of figure 1 depict the dimer rows A, B and C in more detail. The sites on rows B and C are often called hexagonal and cubic sites, respectively (cf e.g. [5–7]). In the present work, this notation is not used because it is not sufficient for the following reasons. Although the sites on *row C* in 4H-SiC and the sites on *row A* in 3C-SiC have identical first and second nearest neighbours, their third neighbour shells are different. Furthermore, on *row C* the distance to the third nearest neighbour is only by a factor of about 1.02 greater than that to the second nearest neighbours, whereas in *row A* this factor is about 1.33. Therefore, the sites on *row C* are not equivalent to those in the cubic polytype. On the other hand, the sites on *row B* in 4H-SiC and on *row A* in 3C-SiC have different second nearest neighbours. The *row B* sites are characteristic for the hexagonal 4H polytype, but they cannot be considered as unique hexagonal sites *per se*. This can be easily demonstrated by comparing with non-equivalent sites in other hexagonal polytypes. For example, in 6H-SiC the corresponding sites have neighbour shells that are different from those in 4H-SiC.

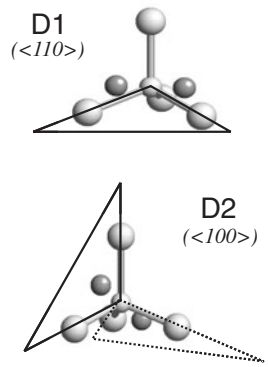

Figure 2. The fundamental structure of D1 and D2 dumbbell interstitials. The light grey spheres and cylinders show the tetrahedron in the ideal lattice. In this example, the central carbon atom is replaced by a C–C dumbbell depicted by two grey spheres. The D1 dumbbell lies in one of the six planes formed by two C–Si bonds. This plane is illustrated by the triangle. The two atoms of the D2 dumbbell are situated in different planes that are perpendicular to each other. In 3C-SiC, the D1 and D2 dumbbells are identical to the ⟨110⟩ and the ⟨100⟩ dumbbells, respectively.

3. Classification of potential elementary defects based on symmetry considerations

3.1. Non-equivalent on-site defects

The higher number of non-equivalent lattice sites in 4H-SiC leads to a greater variety of potential elementary defects than in the 3C polytype. Whereas in 3C-SiC two types of vacancies, V_{Si}^{A} and V_{C}^{A}, exist, in 4H-SiC four different vacancy types, V_{Si}^{B}, V_{Si}^{C}, V_{C}^{B}, and V_{C}^{C}, are present. The subscripts and superscripts denote the vacancy type and the dimer row to which the vacancy belongs, respectively. Similar results are obtained for the antisite defects. In 3C-SiC, the two antisites Si_{C}^{A} and C_{Si}^{A} are found, whereas in 4H-SiC the number of antisites is four (Si_{C}^{B}, Si_{C}^{C}, C_{Si}^{B}, and C_{Si}^{C}).

In covalent materials like Si and SiC, dumbbell self-interstitials are important lattice-site defects since their formation energies may be relatively low. A dumbbell is formed by an interstitial and a lattice atom sharing a lattice site in a split configuration. In a cubic lattice, the dumbbells are oriented parallel to the ⟨110⟩ and to the ⟨100⟩ directions. Due to the polytypism, another classification must be used for SiC. The scheme employed in the present work is based on the consideration of the local environment of the lattice sites. It is valid for 3C-SiC and all hexagonal polytypes, and it may be easily generalized to rhombohedral SiC polytypes. The dumbbell self-interstitials can be classified in two groups, the type 1 (D1) and the type 2 (D2) dumbbells, where the D1 dumbbell lies in one of the six planes formed by two Si–C bonds, and the two atoms of the D2 dumbbell are situated in two perpendicular planes, with each plane being formed by two Si–C bonds. This is illustrated in figure 2 for a dumbbell consisting of two carbon atoms on a carbon site. In 3C-SiC, the D1 and D2 dumbbells are identical to the ⟨110⟩ and the ⟨100⟩ dumbbells, respectively. Whereas in the 3C polytype four non-equivalent D1 dumbbells exist, in 4H-SiC their number is 20. This considerable increase is due to the hexagonal symmetry, which leads to the fact that the D1 dumbbells inside and outside the basal plane are not equivalent. The scheme presented in figure 3 shows more details. The notation for the different D1 dumbbells is explained in the figure caption. Figure 4 depicts the structure of the non-equivalent D2 dumbbells. The number of different D2 dumbbells in 3C- and 4H-SiC is 4 and 12, respectively. In figures 3 and 4, the usual notation for the dumbbells in the cubic polytype (3C-SiC) is given in brackets.

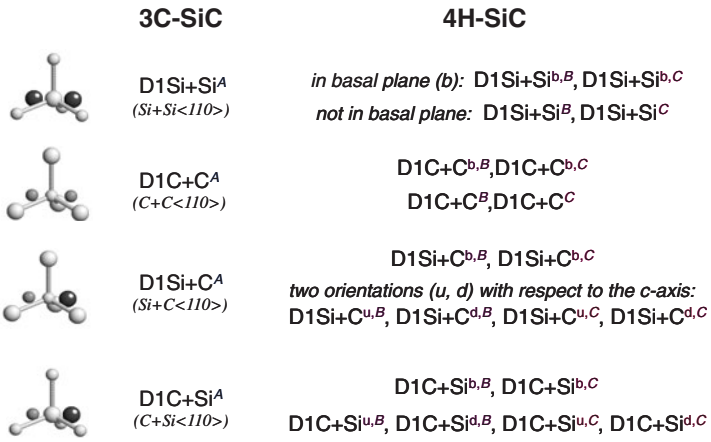

Figure 3. D1 dumbbells in 3C- and 4H-SiC. The four fundamental types are shown schematically. The following notation is used. For example, in the case of D1Si + C^B, C and Si are the original and the additional atoms at the dumbbell site, respectively. The superscript *B* denotes the dimer row in which the dumbbell is situated. Other superscripts are introduced to describe whether the dumbbell lies in the basal plane (superscript b) or to show the orientation (u, d) of a mixed dumbbell which is not in the basal plane. If in a mixed dumbbell the coordinate of the Si atom relative to the *c*-axis is larger (smaller) than that of the C atom, the superscript u (d) is used. The number of non-equivalent D1 dumbbells in 3C-SiC and 4H-SiC is 4 and 20, respectively. Additionally to the general notation valid for cubic as well as hexagonal polytypes, the usual notation for 3C-SiC is given in brackets.

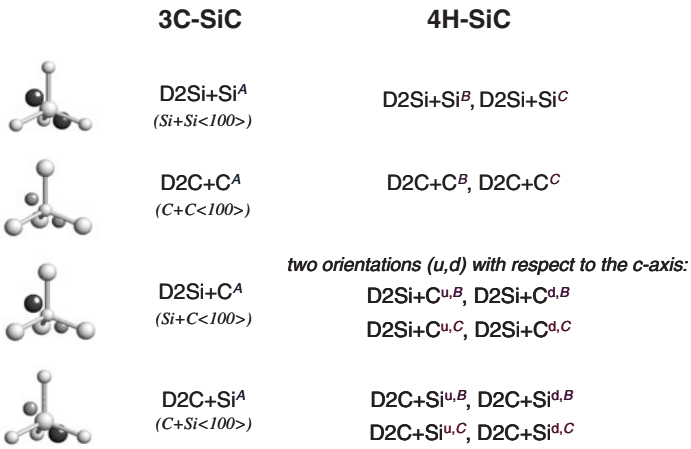

Figure 4. The number of different D2 dumbbells in 3C- and 4H-SiC is 4 and 12, respectively. The schematic representation and the notation are similar to figure 3.

3.2. Elementary defects not related to lattice sites

In both 3C- and 4H-SiC, the number of tetrahedral self-interstitials is four (Si_{TSi}, C_{TC}, Si_{TC}, C_{TSi}). This is due to the fact that in the 4H polytype these interstitials exist only on *row B*. The number of different hexagonal self-interstitials in 3C- and 4H-SiC is two and six, respectively. In the latter case, the hexagonal self-interstitials on *row B* are not equivalent to those that are not on *row B* (Si_H, C_H), i.e. inside a hexagonal Si_3C_3 ring that is not in the basal plane.

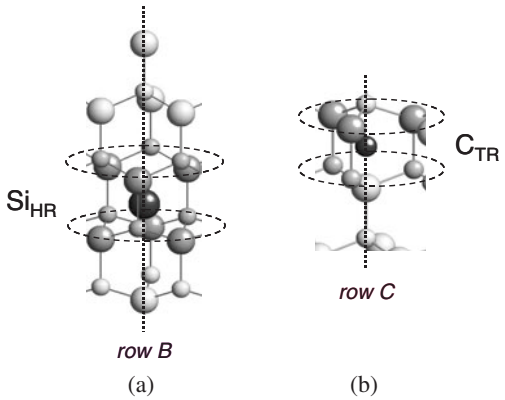

Figure 5. The two highly symmetric self-interstitial structures which are characteristic for the hexagonal polytype. The first defect type consists of a self-interstitial (dark sphere) on *row B* between two hexagonal Si_3C_3 rings (HR). The example shows the Si interstitial Si_{HR} (a). The second type is a self-interstitial on *row C* between a trigonal Si_3 and a trigonal C_3 ring (TR) illustrated in (b) for C_{TR}. The dashed lines mark the hexagonal and trigonal rings. The dotted lines show rows *B* and *C*.

Furthermore, there are two types of interstitials on *row B* that are situated inside the hexagonal Si_3C_3 ring close to carbon (Si_{HC}, C_{HC}) or close to silicon (Si_{HSi}, C_{HSi}) atoms of the same row. Figure 5 depicts two highly symmetric self-interstitial structures that should be found in 4H-, but not in 3C-SiC. Similar defects may also exist in other hexagonal polytypes. The first defect type consists of a self-interstitial on *row B* between two hexagonal Si_3C_3 rings (Si_{HR}, C_{HR}), and the second is an interstitial on *row C* between a trigonal Si_3 and a trigonal C_3 ring (Si_{TR}, C_{TR}).

4. Defect formation energy

The thermodynamically correct definition considers a reference system consisting of a part of a perfect SiC crystal with the same number of Si and C atoms as in the system with the defect. Then, the formation energy for a general neutral defect is given by [8, 5–7]

$$E_D^f = E_D - n_{Si}\mu_{Si} - n_C\mu_C. \tag{1}$$

At 0 K, the difference between the free enthalpy and the energy can be neglected. E_D is the total energy obtained after relaxation of the computational cell with the defect. The number of silicon and carbon atoms in this cell is denoted by n_{Si} and n_C, respectively. For example, in the case of a carbon antisite defect (C_{Si}), n_{Si} is equal to $n_C - 2$. μ_{Si} and μ_C are the chemical potentials of the atoms in the perfect SiC crystal. A simple transformation of equation (1) leads to

$$E_D^f = E_D^{'f} - \tfrac{1}{2}(n_{Si} - n_C)\Delta\mu \tag{2}$$

with

$$E_D^{'f} = E_D - \tfrac{1}{2}(n_{Si} + n_C)\mu_{SiC}^{bulk} - \tfrac{1}{2}(n_{Si} - n_C)(\mu_{Si}^{bulk} - \mu_C^{bulk}) \tag{3}$$

$$\Delta\mu = (\mu_{Si} - \mu_{Si}^{bulk}) - (\mu_C - \mu_C^{bulk}) \tag{4}$$

and

$$\mu_{SiC}^{bulk} = \mu_{Si} + \mu_C = \mu_{Si}^{bulk} + \mu_C^{bulk} - \Delta H_f. \tag{5}$$

The chemical potential of a Si–C pair in bulk SiC is denoted by $\mu_{\mathrm{SiC}}^{\mathrm{bulk}}$; $\mu_{\mathrm{Si}}^{\mathrm{bulk}}$ and $\mu_{\mathrm{C}}^{\mathrm{bulk}}$ are chemical potentials of the atoms in bulk Si and C modifications at 0 K (cubic Si and graphite), respectively, and ΔH_{f} is the formation energy of the solid SiC compound. In the case of $\Delta\mu = 0$, $E_{\mathrm{D}}^{\mathrm{rf}}$ and $E_{\mathrm{D}}^{\mathrm{f}}$ are identical. On the other hand, $\Delta\mu$ is equal to ΔH_{f} and $-\Delta H_{\mathrm{f}}$ under extremely Si-rich and C-rich conditions, respectively. In the former and latter cases, the SiC crystal is connected with a Si or C reservoir, respectively. For example, under Si-rich conditions the SiC crystal has an interface with bulk silicon. Zywietz *et al* [5], Torpo *et al* [6], Eberlein *et al* [7], and Mattausch *et al* [9] employed the above definitions in order to calculate defect formation energies by *ab initio* methods. In Mattausch *et al* [9], only results for Si-rich conditions are given, whereas in the other studies [5–7], data for $\Delta\mu = 0$ as well as for the Si- and C-rich conditions can be found.

An alternative to the calculation of defect formation energies via total energies (equations (1)–(5)) is the use of binding or cohesive energies. This approach must be considered if classical interatomic potentials are used. It was also employed in the *ab initio* calculations of Wang *et al* [10] and Gao *et al* [11, 12]. The formal separation of total energies into contributions resulting from isolated atoms (E_{is}(Si) and E_{is}(C)) and contributions due to the bonds ($E_{\mathrm{D,b}}$), where

$$E_{\mathrm{D}} = E_{\mathrm{D,b}} + n_{\mathrm{Si}}E_{\mathrm{is}}(\mathrm{Si}) + n_{\mathrm{C}}E_{\mathrm{is}}(\mathrm{C}), \tag{6a}$$

$$\mu_{\mathrm{SiC}}^{\mathrm{bulk}} = 2E_{\mathrm{coh}}^{\mathrm{A}}(\mathrm{SiC}) + E_{\mathrm{is}}(\mathrm{Si}) + E_{\mathrm{is}}(\mathrm{C}), \tag{6b}$$

$$\mu_{\mathrm{Si}}^{\mathrm{bulk}} = E_{\mathrm{coh}}^{\mathrm{A}}(\mathrm{Si}) + E_{\mathrm{is}}(\mathrm{Si}), \qquad \mu_{\mathrm{C}}^{\mathrm{bulk}} = E_{\mathrm{coh}}^{\mathrm{A}}(\mathrm{C}) + E_{\mathrm{is}}(\mathrm{C}), \tag{6c}$$

leads to an alternative formulation of equation (3) given by

$$E_{\mathrm{D}}^{\mathrm{rf}} = E_{\mathrm{D,b}} - (n_{\mathrm{Si}} + n_{\mathrm{C}})E_{\mathrm{coh}}^{\mathrm{A}}(\mathrm{SiC}) - \tfrac{1}{2}(n_{\mathrm{Si}} - n_{\mathrm{C}})(E_{\mathrm{coh}}^{\mathrm{A}}(\mathrm{Si}) - E_{\mathrm{coh}}^{\mathrm{A}}(\mathrm{C})), \tag{7}$$

where $E_{\mathrm{coh}}^{\mathrm{A}}$(SiC), $E_{\mathrm{coh}}^{\mathrm{A}}$(Si), and $E_{\mathrm{coh}}^{\mathrm{A}}$(C) are the cohesive energies per atom (superscript A) in bulk SiC, Si and C crystals. The quantity $E_{\mathrm{D,b}}$ denotes the binding or cohesive energy in a computational cell consisting of the SiC lattice with the defect. In the same manner, equation (5) may be reformulated to

$$2E_{\mathrm{coh}}^{\mathrm{A}}(\mathrm{SiC}) = E_{\mathrm{coh}}^{\mathrm{A}}(\mathrm{Si}) + E_{\mathrm{coh}}^{\mathrm{A}}(\mathrm{C}) - \Delta H_{\mathrm{f}}. \tag{8}$$

All previous calculations [10–14] of defect formation energies by binding or cohesive energies were performed for $\Delta\mu = 0$. Furthermore, these investigations did not use the definition given in equation (7), but a relation without the additional term $\frac{1}{2}(n_{\mathrm{Si}} - n_{\mathrm{C}})(E_{\mathrm{coh}}^{\mathrm{A}}(\mathrm{Si}) - E_{\mathrm{coh}}^{\mathrm{A}}(\mathrm{C}))$.

In this work (section 5) the defect formation energy is initially determined employing the same procedure as in [10–14]. Then, the results are transformed to obtain a defect formation energy according to equation (7), using the experimental values for the cohesive energy per atom of bulk Si and C modifications at 0 K ($E_{\mathrm{coh}}^{\mathrm{A}}(\mathrm{Si}) = -4.63$ eV [15], $E_{\mathrm{coh}}^{\mathrm{A}}(\mathrm{C}) = -7.37$ eV [16]), which leads to

$$E_{\mathrm{coh}}^{\mathrm{A}}(\mathrm{Si}) - E_{\mathrm{coh}}^{\mathrm{A}}(\mathrm{C}) = 2.74\ \mathrm{eV}. \tag{9}$$

In order to enable a proper comparison, some *ab initio* data from the literature [10–12] must be also transformed into a form consistent with equation (7) using the relationship defined in equation (9). Another transformation, employing the experimental value for the formation energy of the solid SiC compound ($\Delta H_{\mathrm{f}} \approx 0.7$ eV [17–19]), must be performed, if the literature data are only given for the extremely Si- or C-rich case. It must be emphasized that the use of the experimental values for $E_{\mathrm{coh}}^{\mathrm{A}}$(Si), $E_{\mathrm{coh}}^{\mathrm{A}}$(C), $E_{\mathrm{coh}}^{\mathrm{A}}$(Si) − $E_{\mathrm{coh}}^{\mathrm{A}}$(C) and ΔH_{f} is not unique but it is the most consistent way to obtain a proper comparison of the different literature data since some authors do not report the corresponding theoretical data.

5. Defect stability, energetics and structure

5.1. Computational method

Starting with the ideal defect configuration found by symmetry considerations, classical MD simulations are performed to relax the SiC system at 0 K, for 10 ps, using a rapid quenching scheme. The simulation cell is a rectangular parallelepiped with x-, y-, and z-directions parallel to the $[11\bar{2}0]$, $[\bar{1}100]$ and [0001] axes, respectively. Periodic boundary conditions are applied to all three directions. The cell without any defects contains 1152 and 1920 atoms for 3C- and 4H-SiC, respectively. All simulations are performed at constant volume conditions. In the case of dumbbell self-interstitials, before the relaxation simulation, the distance between the two atoms of the dumbbell is varied to obtain the configuration with the lowest formation energy.

The reliability of results obtained by MD simulations depends decisively on the quality of the interatomic potential employed. In previous studies on elementary defects in 3C-SiC, the potentials of Tersoff [20, 21, 13, 11, 22] and Gao–Weber [1] were used. The comparison of these results is complicated by the fact that different parameter sets for the Tersoff function [20, 21, 13] and the Tersoff cut-off radii [20, 11, 22] may be employed. Furthermore, it has been found that some previous results based on using the Tersoff potential were not correct. Therefore, the calculations of the structure and energetics of elementary defects in 3C-SiC have been repeated. The results are given in the appendix, together with *ab initio* data from the literature, along with a more detailed discussion. The *ab initio* data obtained by different groups show a reasonable agreement for vacancies and antisites, but not for interstitials. Determining the reason for this disagreement is beyond the scope of the present study. However, because of the agreement for vacancies and antisites, it is unlikely that the difference is due to the transformation of the literature data that is described at the end of section 4. On the other hand, the data determined by different classical potentials also do not agree well.

The present comparative study employs the Gao–Weber potential [1] that was parameterized to bulk properties of 3C-SiC (lattice constant, cohesive energy, etc) and to the results of *ab initio* calculations [11] for native defects in 3C-SiC. The appendix contains a detailed comparison of these data with the corresponding results obtained by the Gao–Weber potential. It shows that the potential reproduces the bulk properties very well. The values of the formation energies calculated for most defects in 3C-SiC are comparable to the *ab initio* results of [11], although some differences exist. In particular the vacancy formation energies are smaller than those obtained by *ab initio* calculations. However, *ab initio* calculations and the classical MD simulations with the Gao–Weber potential as well as the COP3/TP1,3 parametrizations (cf tables A.1–A.3) of the Tersoff potential, yield the result that, of all the C interstitials, the ⟨100⟩-oriented C + C dumbbell has the lowest formation energy. This is consistent with experimental investigations [25]. For 4H-SiC, the accuracy of the Gao–Weber potential is similar to that for 3C-SiC, since both polytypes are characterized by fourfold-coordinated atoms, and the only difference consists in the second and the following neighbour shells. Like the different versions of the Tersoff potential, the Gao–Weber potential considers only short-range interactions with a cut-off between the first and the second neighbour shells of an ideal lattice site. Therefore, for 4H-SiC the Gao–Weber potential predicts the same bulk properties as for 3C-SiC. It cannot reproduce the slight deviations (of the order of 1% of the lattice constant) from the ideal tetrahedral structure observed for the 4H polytype [26]. Therefore, one may expect that in the following results the influence of polytypism on the stability, energetics and structure of elementary defects in SiC is rather underestimated than overestimated, since this effect is exclusively due to the different neighbour shells of the corresponding defects.

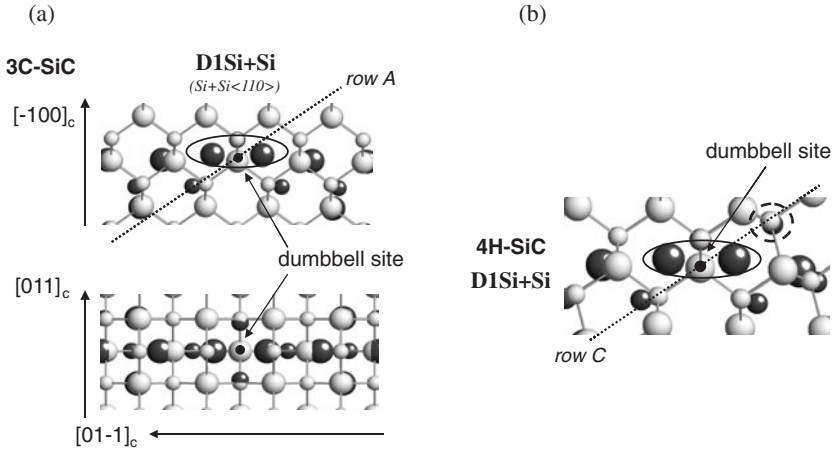

Figure 6. (a) The spatial structure of the dumbbell D1Si + Si in 3C-SiC. The light grey spheres and cylinders depict atoms and bonds of the ideal lattice. Atoms, the positions of which deviate from that in the ideal crystal, are marked by dark spheres. The upper figure shows a view into the $[0\bar{1}\bar{1}]_c$ direction. The atoms of the dumbbell are marked by the ring. The dumbbell as well as *row A* are situated in the plane of the figure. A view into the $[100]_c$ direction, which is perpendicular to $[0\bar{1}\bar{1}]_c$, is depicted in the lower figure. (b) The structure of the dumbbell D1Si + Si^C in 4H-SiC. The dumbbell as well as *row C* lie in the plane of the figure. One atom is marked by a dashed ring. This is the third nearest neighbour of the dumbbell site which has another position than in the corresponding dumbbell structure shown in (a).

5.2. Results and discussion

For defects related to lattice sites, the comparison between formation energies in 4H- and 3C-SiC is shown in table 1. The energetics of vacancies and antisites is nearly independent of the polytype since significant lattice deformations are found only in the immediate vicinity of these simple defects.

The structure of the D1 dumbbells is rather complex and anisotropic as illustrated in figure 6(a) for D1Si + Si in 3C-SiC. Therefore, for such interstitials one may expect more differences between 3C- and 4H-SiC than for vacancies and antisites. In particular, this concerns the Si–Si dumbbells and the mixed dumbbells on carbon sites. On the other hand, the formation energies of C–C dumbbells and mixed dumbbells on silicon sites do not depend so strongly on the polytype. These results demonstrate the effect of the atomic size which can lead to significant lattice deformations. In *row C*, the Si–Si dumbbell in the basal plane (D1Si + $Si^{b,C}$) is similar to that in the 3C polytype, but the corresponding dumbbell in *row B* is different. This is due to the fact that the dumbbell sites in rows *A* and *C* have the same first nearest and second nearest neighbours, whereas the site in *row B* differs already by the second nearest neighbour. On the other hand, the formation energy of the Si–Si dumbbell in *row C*, which is outside the basal plane (D1Si + Si^C), deviates from that for the corresponding dumbbell in 3C-SiC. This result may be explained by the influence of the third nearest neighbour atom of the dumbbell site in *row C*. As already mentioned above, the distance to this atom is only a factor of about 1.02 greater than that to the second nearest neighbours. In the case of D1Si + Si^C, the third nearest neighbour atom is very close to the anisotropic dumbbell structure and therefore has an important influence on lattice relaxation, which is in contrast to D1Si + $Si^{b,C}$. Figure 6(b) shows the structure of D1Si + Si^C. Its formation energy is smaller than that of the corresponding dumbbell in 3C-SiC (figure 6(a)). This indicates

Table 1. Comparison between defect formation energies (in eV) in 4H- and 3C-SiC, for the defects related to lattice sites. The data in this and the following table were calculated using the Gao–Weber potential [1] and the thermodynamically correct definition of the formation energy for $\Delta\mu = 0$ (cf equation (7)). The dumbbell notation is explained in figures 3 and 4. The spatial defect structure was analysed in each case. In some cases, the deviation from the ideal dumbbell configuration is considerable. Strong and very strong deviations are marked by asterisks and crosses, respectively.

4H-SiC			3C-SiC	
Defect type	Row B	Row C	Row A	Defect type
		Vacancies		
V_{Si}	4.67	4.68	4.67	V_{Si}
V_C	1.39	1.40	1.39	V_C
		Antisite defects		
C_{Si}	4.43	4.44	4.43	C_{Si}
Si_C	5.04	5.06	5.04	Si_C
		D1 dumbbells		
D1Si + Si^b	3.46	3.72	3.72	D1Si + Si (Si + Si⟨110⟩)
D1Si + Si	2.96	3.06		
D1C + C^b	4.72	4.68	4.67	D1C + C (C + C⟨110⟩)
D1C + C	4.66	4.75		
D1Si + C^b	Not stable	3.40*		
D1Si + C^u	3.01*	2.49*	3.54*	D1Si + C (Si + C⟨110⟩)
D1Si + C^d	5.58*	6.03+		
D1C + Si^b	5.34	5.32		
D1C + Si^u	5.53	5.35	5.32	D1C + Si (C + Si⟨110⟩)
D1C + Si^d	5.30	5.59		
		D2 dumbbells		
D2Si + Si	4.16	4.18	4.15	D2Si + Si (Si + Si⟨100⟩)
D2C + C	4.41	4.43	4.41	D2C + C (C + C⟨100⟩)
D2Si + C^u	4.18*	2.83+	6.06+	D2Si + C (Si + C⟨100⟩)
D2Si + C^d	6.07+	6.11+		
D2C + Si^u	4.65	4.81	4.79	D2C + Si (C + Si⟨100⟩)
D2C + Si^d	4.78	4.81		

better conditions for lattice relaxation. The mixed dumbbell on the carbon site is illustrated in figure 7. Of the different D1 dumbbells, this structure is the most complex. It may be also considered as a defect consisting of two Si atoms and one C atom occupying the region of a Si–C dimer in the ideal lattice. The three atoms lie in the same plane. Figure 7 demonstrates the strong dependence of energetics on the spatial defect structure of each polytype. The most compact defects, D1Si + $C^{u,B}$ and D1Si + $C^{u,C}$, have the lowest formation energies, which are smaller than the formation energies of the corresponding defects in 3C-SiC. On the other hand, the formation energy of the complicated anisotropic structures (D1Si + $C^{d,B}$ and D1Si + $C^{d,C}$) is generally higher.

The D2 dumbbells are not as anisotropic as the D1 dumbbells, but show a three-dimensional structure (cf figure 8). This may be the reason why the results for the two polytypes are similar in many cases. However, this does not hold for the D2Si + C dumbbells. In general the relaxed structure of D2Si + C strongly deviates from the ideal configuration (cf figures 2

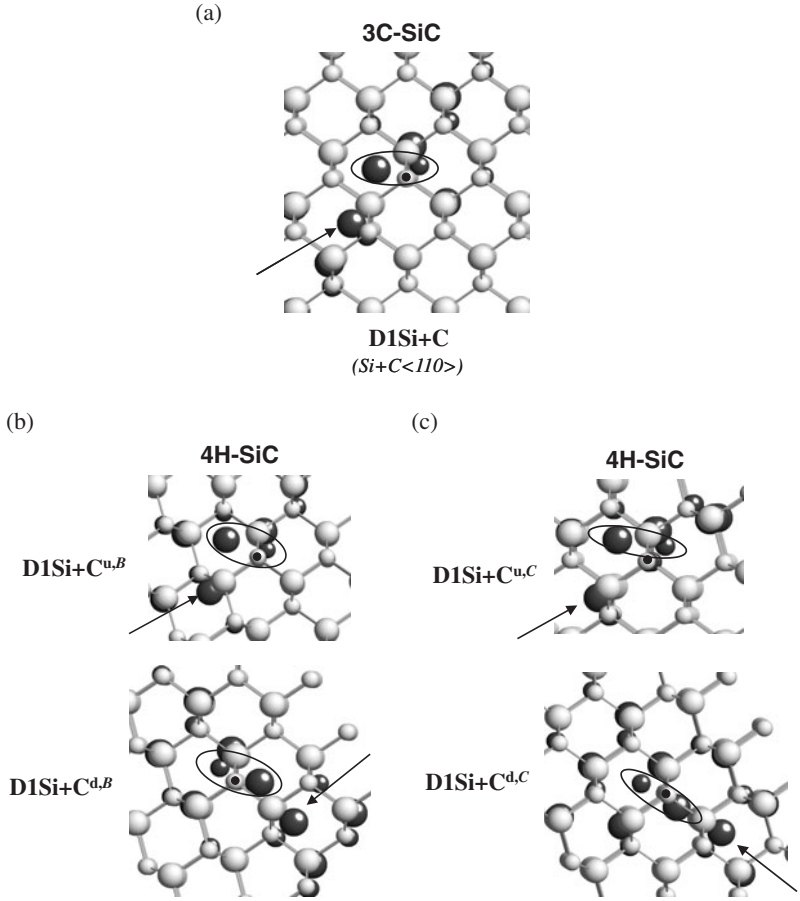

Figure 7. Structures of the mixed dumbbell D1Si + C in the 3C (a) and the 4H polytype (b), (c). The black dot and the ring mark the dumbbell site and the two atoms forming the dumbbell, respectively. The defect may be also considered as a complex of two Si atoms and one C atom occupying the region of a Si–C dimer in the ideal lattice. The third atom is marked by an arrow. The three atoms lie in the same plane, which is identical to the plane of the figure. The compact structures in (b) and (c) have the lowest formation energies (cf table 2).

and 4). With the exception of D2Si + $C^{u,B}$, the position of the dumbbell atoms is not exactly within the corresponding planes. The structure of D2Si + C in 3C-SiC and of D2Si + $C^{d,B}$ and D2Si + $C^{d,C}$ is very similar, leading to formation energies that are nearly equal. On the other hand, D2Si + $C^{u,B}$ is close to the ideal D2 configuration, whereas D2Si + $C^{u,C}$ shows the most irregular structure. Therefore, their energetics differs significantly from that of the other D2Si + C. It should be mentioned that non-regular D2Si + C structures are also observed if the Tersoff interatomic potential is employed. Therefore, within the framework of classical potential methods it cannot be clarified whether the particular structure of D2Si + C is an artefact due to the potential.

In 3C- and 4H-SiC the first, the second and the third neighbour shells of the tetrahedral interstitial site are identical; thus the formation energy in both polytypes is almost the same, as shown in table 2. On the other hand, figure 9 illustrates that these tetrahedral interstitials have a rather extended three-dimensional structure with significant lattice deformations. Of the hexagonal interstitials, only the carbon interstitial is stable. It is a rather compact defect

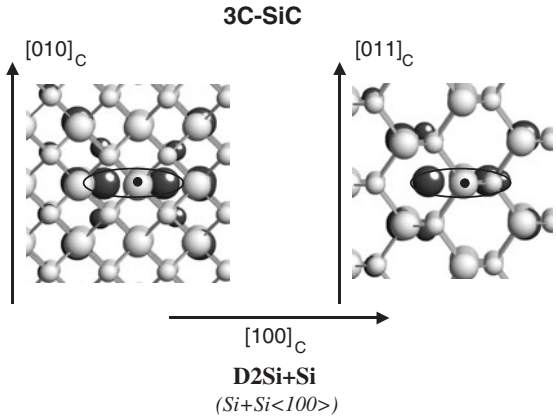

Figure 8. D2Si + Si in 3C-SiC. The lattice deformations around this defect do not show a pronounced anisotropy.

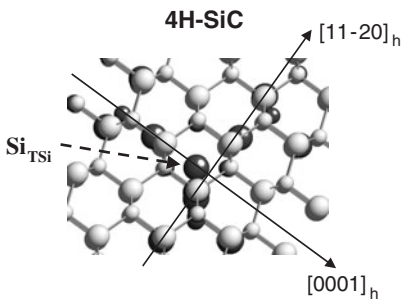

Figure 9. The Si interstitial on tetrahedral position, Si_{TSi}, in 4H-SiC. The two directions $[11\bar{2}0]_h$ and $[0001]_h$ lie in the plane of the figure.

as shown in figure 10(a). This may be the reason why the influence of polytypism on the structure and energetics of this defect is negligible (cf table 2). Figure 10(b) depicts the relatively isotropic structure of carbon interstitial between two hexagonal Si_3C_3 rings. Both the Si_{HR} and the C_{HR} interstitial are stable. On the other hand, only the carbon interstitial between the Si_3 and the C_3 trigonal ring is stable, but it has a large formation energy.

In the case of $\Delta\mu = 0$, the following energy hierarchy is obtained for interstitials in 4H-SiC. The C interstitial with the lowest formation energy is $D2C + C^B$, followed by $D1C + C^B$ and $D2C + Si^{u,B}$. The corresponding defects in 3C-SiC show the same sequence. The Si interstitial with the lowest formation energy is $D1Si + C^{u,C}$, followed by Si_{TC} and $D2Si + C^{u,C}$. This sequence is different to that in 3C-SiC. For vacancies and antisite defects, the energy hierarchy in 3C- and 4H-SiC is identical. In both cases the carbon vacancy and carbon on silicon site have a lower formation energy than the corresponding silicon defects.

Table 3 compares the limited number of available *ab initio* data [5–7] on elementary defects in 4H-SiC with corresponding values for 3C-SiC. The formation energy of the compact defects investigated shows a weak polytype and site dependence. This is consistent with the results of present classical MD simulations using the Gao–Weber potential.

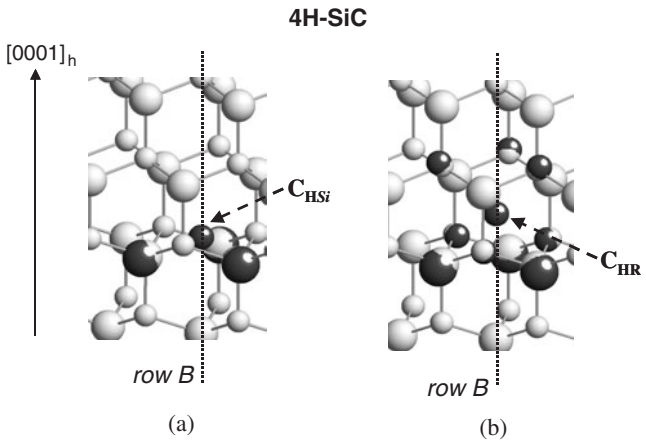

Figure 10. The structure of the interstitials C_{HSi} (a) and C_{HR} (b) in 4-SiC.

Table 2. Comparison between the energetics of defects in 4H- and 3C-SiC, for interstitials not related to lattice sites.

4H-SiC			3C-SiC	
Defect type	Row B	Row C	Row A	Defect type
Tetrahedral interstitials				
Si_{TSi}	5.38		5.39	Si_{TSi}
Si_{TC}	2.60		2.60	Si_{TC}
C_{TSi}	5.69		5.69	C_{TSi}
C_{TC}	5.37		5.38	C_{TC}
Hexagonal interstitials				
Si_H	Not stable			
Si_{HSi}	Not stable		Not stable	Si_H
Si_{HC}	Not stable			
C_H	5.15			
C_{HSi}	5.15		5.15	C_H
C_{HC}	5.15			
Interstitials between two hexagonal Si_3C_3 rings				
Si_{HR}	3.39			
C_{HR}	4.85			
Interstitials between Si_3 and C_3 trigonal rings				
Si_{TR}	Not stable			
C_{TR}	6.26			

6. Conclusions

A comparative study of elementary defects in 3C- and 4H-SiC was performed. It is based on a novel defect classification scheme that is valid for both cubic and hexagonal polytypes and may be easily generalized to rhombohedral SiC. The number of potential non-equivalent defects in 4H-SiC obtained from this classification is considerably higher than in 3C-SiC. Although the fundamental defect types are mostly similar, the hexagonal symmetry leads

Table 3. Defect formation energies for 4H-SiC obtained by *ab initio* calculations [5–7], in comparison with corresponding values for 3C-SiC. The *ab initio* data of [5] were determined by two methods: LDA- and LSDA-DFT. The latter results are given in brackets.

4H-SiC							3C-SiC				
	Row *B*			Row *C*			Row *A*				
Defect type	[5]	[6]	[7]	[5]	[6]	[7]	[10]	[5]	[11]	[9]	Defect type
V_{Si}	8.23 (7.97)	8.26		8.31 (8.05)	8.37		8.17	8.69 (8.45)	8.01	7.8	V_{Si}
V_C	4.15 (4.15)	4.21		4.03 (4.03)	4.07		4.53	4.30 (4.30)	4.11	4.5	V_C
C_{Si}		3.57	3.60		3.52	3.60	3.84		4.06		C_{Si}
Si_C		4.25	4.15		4.29	4.15	4.56		4.46		Si_C
D2C + C			6.90			6.70			4.53	7.0	D2C + C (C + C⟨100⟩)

to a diversification. After a detailed discussion of the methods for determining the defect formation energy by classical-potential and *ab initio* calculations, the available data for 3C-SiC were reviewed. The data determined by different theoretical methods and/or different authors do not agree well. The stability, structure and energetics of the large number of potential non-equivalent defects in 4H-SiC were investigated by classical MD simulations using the Gao–Weber potential. Most of the potential defects in 4H-SiC were found to be stable. The structure and energetics of some complex and anisotropic defects, in particular for the dumbbells D1Si + Si and D1Si + C, as well as for D2Si + C, differ considerably from that in 3C-SiC. This may be due to the important role of lattice deformation beyond the first nearest neighbour shell, and the fact that the spatial distribution of such deformations is strongly dependent on the polytype structure. The interstitials between hexagonal and trigonal rings are characteristic for hexagonal SiC, which do not exist in the cubic polytype. The polytypism does not have a significant influence on the structure and the energetics of the more compact and isotropic defects, like vacancies, antisites, hexagonal interstitials, and many D1 and D2 dumbbells. The compact defects are characterized by relatively small deformations in the immediate vicinity of the defect site so that polytypism does not play any role. On the other hand, for isotropic defects the deformations beyond the first nearest neighbour shell are not as strongly dependent on the polytype structure as in the case of the anisotropic defects. Despite their complexity, the tetrahedral interstitials have very similar properties in 3C- and 4H-SiC, since their first, second and third nearest neighbour shells are equal. In 3C- and 4H-SiC, the energy hierarchy of carbon interstitials, vacancies and antisites as well as of silicon vacancies and antisites is very similar, whereas for silicon interstitials differences were found. The energy hierarchy of the defects is related to their thermal stability. Detailed investigations on this important topic will be the subject of future investigations. The interatomic potential used in this work is characterized by a relatively short interaction range, and thus the present results should rather underestimate than overestimate the differences between the polytypes.

Appendix: The energetics of elementary defects in 3C-SiC

Table A.1 summarizes the energetics of neutral defects in 3C-SiC. The data were calculated using the thermodynamically correct definition of the formation energy for $\Delta\mu = 0$ (cf equations (3) and (7)). The *ab initio* data were obtained from the literature. If necessary, they were transformed as described at the end of section 4. Note that the numbers in the fifth column were taken from a figure in [9], so they may slightly differ from the original

Table A.1. Summary of formation energies (eV) of neutral defects in 3C-SiC. For the different versions of the Tersoff potential and their acronyms, the reader is referred to tables A.2(a) and (b). The letter 'X' marks cases where the defect is not stable. The notation of the dumbbells is illustrated in figures 3 and 4. In [5] the data were obtained by LDA- and LSDA-DFT. The latter results are given in brackets.

					Tersoff potential									
	Ab initio				COP1			COP2			COP3			
Defect type	[10]	[5]	[11]	[9]	TP1	TP2	TP3	TP1	TP2	TP3	TP1	TP2	TP3	Gao pot. [1]
V_{Si}	8.17	8.69 (8.45)	8.01	7.8	3.14	7.80	7.64	3.14	7.80	7.64	3.14	7.80	7.64	4.67
V_C	4.53	4.30 (4.30)	4.11	4.5	3.89	4.19	4.22	3.88	4.08	4.10	3.88	4.08	4.10	1.39
C_{Si}	3.84		4.06		2.29	2.42	2.66	2.19	2.33	2.57	2.19	2.33	2.57	4.43
Si_C	4.56		4.46		4.34	6.09	6.60	3.37	4.01	4.10	3.37	4.01	4.10	5.04
Si + Si⟨110⟩				9.4	15.9	18.1	18.5	15.3	15.0	16.9	12.5	12.1	12.6	3.72
C + C⟨110⟩			4.69	13.3	7.88	8.64	X	7.68	8.32	8.57	8.06	9.13	9.34	4.67
Si + C⟨110⟩					X	X	X	12.7*	12.6*	13.1*	11.5*	12.2*	12.5*	3.54*
C + Si⟨110⟩			4.65		X	13.4	13.4	X	X	X	12.0	11.8	12.3	5.32
Si + Si⟨100⟩			7.95		14.7	17.2	17.5	14.6	16.5	16.7	9.86*	10.2	10.4	4.15
C + C⟨100⟩			4.53	7.0	5.95	10.3	10.2	5.32	8.39*	8.19*	5.32	8.34*	8.15*	4.41
Si + C⟨100⟩			8.68		X	9.45*	X	X	13.5^+	13.8^+	9.34*	11.6^+	11.6^+	6.06^+
C + Si⟨100⟩			4.96	7.4	9.24	X	12.3	9.14	8.64	8.73	6.69	8.23	8.28	4.79
Si_{TSi}	13.6		7.34		15.4	18.7	19.0	19.9	17.9	18.8	14.8	15.7	16.8	5.39
Si_{TC}	13.3		4.80		17.6	17.9	18.8	17.0	16.0	16.7	13.2	11.6	12.4	2.60
C_{TSi}	9.97		7.21	9.5	5.37	4.47	4.50	4.37	4.47	4.50	9.26	17.1	16.2	5.69
C_{TC}	12.4		8.28 7.78 [12, 1]	11.0	7.18	7.53	7.78	7.53	14.1	15.3	13.8	11.6	12.6	5.38
Si_H					17.4*	18.0*	X	15.3	14.7	15.2	13.9*	13.2*	13.8*	X
C_H				8.9	4.72	7.94	X	12.5	11.1	11.9	12.5	11.2	11.9	5.15

data. The method given in section 5.1 has been applied to determine the formation energies using the classical interatomic potentials. Although data for the Tersoff potential were already published [13, 14, 11, 12], a careful check of the data indicated that some results from previous investigations were not correct since they employed the experimental value for the lattice parameter instead of that obtained by the different versions of the Tersoff potential. Therefore, many of the calculations have been repeated. The parameter values for the Tersoff function and for the cut-off radii are given in tables A.2(a) and (b). Table A.3 compares the experimental data for the lattice parameter and the cohesive energy per atom with those obtained by the Gao–Weber potential and the different versions of the Tersoff potential.

For vacancies and antisite defects the *ab initio* results do not differ very much. In the case of interstitials, there is no satisfactory agreement between the *ab initio* values published by different authors. Finding the reasons for the disagreement is beyond the scope of the present work. The Gao–Weber potential [1] used in the present comparative study was parameterized to the *ab initio* data given in [11]. Therefore, for most defects, the formation energies obtained by the Gao–Weber potential are comparable with those *ab initio* data, although some differences exist. In particular, the vacancy formation energies are smaller than those obtained by *ab initio* calculations. In general, the formation energies for Si interstitials obtained by the Gao–Weber potential are significantly lower than those obtained for the Tersoff potential. In many cases, this also holds for the formation energy of C interstitials. Furthermore, the Si and C interstitials

Table A.2. Different versions of the Tersoff potential for SiC. (a) Values for the parameters in the Tersoff function. The notation of the parameters is the same as in [20, 21, 13]. (b) Values for the cut-off radii. The notation is the same as in [20, 21, 13, 22, 11].

(a)	TP1 [20]			TP2 [21]			TP3 [13]		
	Parameters of the bonds								
	Si–Si	C–C	Si–C	Si–Si	C–C	Si–C	Si–Si	C–C	Si–C
A (eV)	1830.8	1393.6	$\sqrt{A_{\mathrm{Si-Si}}A_{\mathrm{C-C}}}$	TP1	1544.8	$\sqrt{A_{\mathrm{Si-Si}}A_{\mathrm{C-C}}}$	TP1	TP2	$\sqrt{A_{\mathrm{Si-Si}}A_{\mathrm{C-C}}}$
λ (Å^{-1})	2.4799	3.4879	$\frac{(\lambda_{\mathrm{Si-Si}}+\lambda_{\mathrm{C-C}})}{2}$		3.4653	$\frac{(\lambda_{\mathrm{Si-Si}}+\lambda_{\mathrm{C-C}})}{2}$			$\frac{(\lambda_{\mathrm{Si-Si}}+\lambda_{\mathrm{C-C}})}{2}$
B (eV)	471.18	346.74	$\sqrt{B_{\mathrm{Si-Si}}B_{\mathrm{C-C}}}$		389.63	$\sqrt{B_{\mathrm{Si-Si}}B_{\mathrm{C-C}}}$			$\sqrt{B_{\mathrm{Si-Si}}B_{\mathrm{C-C}}}$
μ (Å^{-1})	1.7322	2.2119	$\frac{(\mu_{\mathrm{Si-Si}}+\mu_{\mathrm{C-C}})}{2}$		2.3064	$\frac{(\mu_{\mathrm{Si-Si}}+\mu_{\mathrm{C-C}})}{2}$			$\frac{(\mu_{\mathrm{Si-Si}}+\mu_{\mathrm{C-C}})}{2}$
χ	1.0	1.0	0.9776		1.0	1.0086			1.0121
ω	1.0	1.0	1.0		1.0	1.0			1.0
	Parameters for the central atom used in the calculation of the bond-order parameter								
	Si		C	Si		C	Si		C
β	1.0999×10^{-6}		1.5724×10^{-7}	1.1×10^{-6}		4.1612×10^{-6}	TP2		TP2
n	0.787 34		0.727 51	TP1		0.990 54			
c	100 390.0		38 049.0			19 981.0			
d	16.218		4.3484	16.217		7.034			
h	−0.598 26		−0.570 58	−0.598 25		−0.339 53			−0.399 53
(b)	COP1 [20]			COP2 [22]			COP3 [11]		
	Si–Si	C–C	Si–C	Si–Si	C–C	Si–C	Si–Si	C–C	Si–C
R (Å)	2.7	1.8	2.204 54	2.60	1.93	2.36	2.204 54	2.204 54	2.204 54
S (Å)	3.0	2.1	2.509 98	2.80	2.13	2.56	2.509 98	2.509 98	2.509 98

Table A.3. Cohesive energy per atom and nearest neighbour distance derived from different versions of the Tersoff potential and from the Gao–Weber potential in comparison with experimental data.

	Tersoff potential				
3C-SiC	TP1	TP2	TP3	Gao–Weber pot. [1]	Exp. data
$E_{\mathrm{coh}}^{\mathrm{A}}$ (eV/atom)	−6.16	−6.43	−6.46	−6.41	−6.34 [23]
nn distance (Å)	1.87	1.85	1.85	1.89	1.89 [24]

have similar formation energies if the Gao–Weber potential is employed, whereas in the case of the Tersoff potential, the formation energy of the Si interstitial is generally higher. The spatial defect structure of each defect has been also analysed. In some cases, the deviation from the ideal dumbbell configuration is considerable. In table A.1, strong and very strong deviations are marked by asterisks and crosses, respectively.

References

[1] Gao F and Weber W J 2002 *Nucl. Instrum. Methods Phys. Res.* B **191** 504
[2] Pirouz P and Yang J W 1992 *Ultramicroscopy* **51** 189

[3] Powell J A, Pirouz P and Choyke W J 1992 *Semiconductor Interfaces, Microstructures and Devices: Properties and Applications* ed Z C Feng (Bristol: Hilger) p 257
[4] Verma A and Krishna P 1966 *Polymorphism and Polytypism in Crystals* (New York: Wiley)
[5] Zywietz A, Furthmüller J and Bechstedt F 1999 *Phys. Rev.* B **59** 15166
[6] Torpo L, Marlo M, Staab T E M and Nieminen R M 2001 *J. Phys.: Condens. Matter* **13** 6203
[7] Eberlein T A G, Fall C J, Jones R, Briddon P R and Öberg S 2002 *Phys. Rev.* B **65** 184108
[8] Zhang S B and Northrup J E 1991 *Phys. Rev. Lett.* **67** 2339
[9] Mattausch A, Bockstedte M and Pankratov O 2001 *Mater. Sci. Forum* **353–356** 323
[10] Wang C, Bernholc J and Davis R F 1988 *Phys. Rev.* B **38** 12752
[11] Gao F, Bylaska E J, Weber W J and Corrales L R 2001 *Nucl. Instrum. Methods Phys. Res.* B **180** 286
[12] Gao F, Bylaska E J, Weber W J and Corrales L R 2001 *Phys. Rev.* B **64** 245208
[13] Huang H, Ghoniem N M, Wong J K and Baskes M I 1995 *Modelling Simul. Mater. Sci. Eng.* **3** 615
[14] Malerba L, Perlado J M, Colombo L and Diaz de la Rubia T 2000 *Mass Transport in Inorganic Materials—Fundamentals to Devices* ed P Vincenzini and V Buscaglia (Faenza: Techna srl) pp 1385–93
[15] Chang K J and Cohen M L 1987 *Phys. Rev.* B **35** 8196
[16] Furthmüller J, Hafner J and Kresse G 1994 *Phys. Rev.* B **50** 15606
[17] Kubaschewski O and Alcock C B 1979 *Metallurgical Thermochemistry* (Oxford: Pergamon)
[18] Holleman-Wiberg 1985 *Lehrbuch der Anorganischen Chemie* (Berlin: W. de Gruyter)
[19] Chase M W Jr (ed) 1998 *NIST-JANAF Thermochemical Tables* 4th edn *J. Phys. Chem. Ref. Data, Monograph* **9** 1–1951
[20] Tersoff J 1989 *Phys. Rev.* B **39** 5566
Tersoff J 1990 *Phys. Rev.* B **41** 3248
Tersoff J 1988 *Phys. Rev.* B **38** 9902
Tersoff J 1988 *Phys. Rev. Lett.* **61** 2879
[21] Devanathan R, Diaz de la Rubia T and Weber W J 1998 *J. Nucl. Mater.* **253** 47
[22] Tang M and Yip S 1995 *Phys. Rev.* B **52** 15150
[23] Wagman D D, Evans W H, Parker V B, Halow I, Baily S M and Schumm R H 1968 Selected values of chemical thermodynamics properties, tables for the first thirty-four elements in the standard order of arrangement *Natl. Bur. of Stand. Tech. Note No.* 270-3 (Washington, DC: US Government Printing Office)
[24] Madelung O, Schulz M and Weiss H (ed) 1982 *Physics of Group IV Elements and III–V Compounds* (*Landolt-Börnstein Tables* vol 17a) (Berlin: Springer)
[25] Steeds J W, Evans G A, Furkert S, Ley L, Hundhausen M, Schulz M and Pensl G 2003 *Mater. Sci. Forum* **433–436** 305
[26] Harris G L (ed) 1995 *Properties of Silicon Carbide* (*EMIS Datareviews Series No 13*) (London: INSPEC)